10-2017

Eulerian-Based Virtual Visual Sensors to Measure Dynamic Displacements of Structures

Ali Shariati
University of Delaware

Thomas Schumacher
Portland State University, thomas.schumacher@pdx.edu

Eulerian-Based Virtual Visual Sensors to Measure Dynamic Displacements of Structures

Ali Shariati[1,*] and Thomas Schumacher[2]

[1] Civil and Environmental Engineering, University of Delaware, Newark, DE 19716, USA; E-mail: alish@udel.edu

[2] Civil and Environmental Engineering, Portland State University, Portland, OR 97201, USA; E-mail: thomas.schumacher@pdx.edu

***** Author to whom correspondence should be addressed; E-Mail: alish@udel.edu;
Tel.: +1-443-449-1414; Fax: +1-302-831-3640.

Abstract: Vibration measurements provide useful information about a structural system's dynamic characteristics and are used in many fields of science and engineering. Here, we present an alternative non-contact approach to measure dynamic displacements of structural systems using digital videos. The concept is that intensity measured at a pixel with a fixed (or Eulerian) coordinate in a digital video can be regarded as a virtual visual sensor (VVS). The pixels in the vicinity of the boundary of a vibrating structural element contain useful frequency information, which we have been able to demonstrate in earlier studies. Our ultimate goal, however, is to be able to compute dynamic displacements, i.e. actual displacement amplitudes in the time domain. In order to achieve that we introduce the use of simple black-and-white targets (BWT) that are

mounted to locations of interest on the structure. By using these targets, intensity can be directly related to displacement, turning a video camera into a simple, computationally inexpensive, and accurate displacement sensor with notably low signal-to-noise ratio (SNR). We show that subpixel accuracy with levels comparable to computationally-expensive block matching algorithms can be achieved using the proposed targets. Our methodology can be used for laboratory experiments, on real structures, and additionally we see educational opportunities in the K-12 classroom. In this paper we introduce the concept and theory of the proposed methodology, present and discuss a laboratory experiment to evaluate the accuracy of the proposed BWT target, and discuss the results from a field test of an in-service bridge.

Keywords: Vibration; Dynamic displacement; Structural health monitoring; Digital video; Virtual visual sensor; Eulerian coordinate; Black-and-white target; Subpixel accuracy.

1 Introduction

Structural vibrations contain important information about a structural system's dynamic characteristics. Changes over time in the vibration response can be caused by alterations in the loading, boundary conditions, or degradation of the structural system. As such, structural health monitoring (SHM) has emerged as a modern asset management support tool to help owners and managers make more informed decisions regarding repair, optimal intervention, and management of lifeline assets such as bridges during regular service and after extreme events such as natural disasters. Vibration-based SHM methods use dynamic characteristics such as natural frequencies and mode shapes to detect the occurrence of damage and estimate its location and severity [1]–[3]. A critical step in this process is the gathering of the vibration data using sensors or sensor networks.

The ultimate goal is to have a sensing system that produces objective, quantitative, and accurate data, inexpensively. Conventional contact-type sensors such as strain gages or accelerometers that are attached to specific locations of a structure are capable of measuring the response at that specific point. Accessibility of the member of interest combined with wiring issues in addition to high local-only sensitivity are some drawbacks of conventional sensors, which have urged innovation to develop non-contact sensors. On the other hand, laser interferometry instruments are reliable but comparatively expensive as they use sophisticated equipment and require specialized trained operators [4]. Photogrammetry methods have been used in the measurement of static displacements and strains in bridges. More recently, digital image correlation (DIC) and other block matching algorithms [5],[6] that use digital video data to measure static displacement fields with high accuracy have been explored [7]–[10]. However, the computational cost of these methods is relatively high. Efficient yet accurate non-contact methods are needed that are computationally inexpensive and work with standard digital video cameras.

In this paper, we propose a simple alternative way to measure structural vibrations using Eulerian-based virtual visual sensors (VVS), for which the fundamental basis we have developed earlier [11]–[13] We show that for a black-and-white target (BWT), a linear intensity-displacement relationship exists for a patch of pixels on the boundary of the target. We refer to this as intensity-to-displacement transform (IDT). It should be noted that this same transform can also be applied without using BTWs, for example to the edge of a structural member where a distinct boundary between the member and the background exists. Fig. 1 illustrates the concept of our proposed methodology: a BWT target is attached to a location of interest. From the digital video extracted from the camera, a VVS located on the BWT is selected. The change of intensity is recorded over

time (green curve) and by employing a linear transformation (= IDT) converted to actual displacement (blue curve). Also shown is a frequency analysis (red curve), which can be obtained directly from the intensity time history by using a Fast Fourier transform (FFT). The focus of this paper is on how to compute displacement time histories (blue curve).

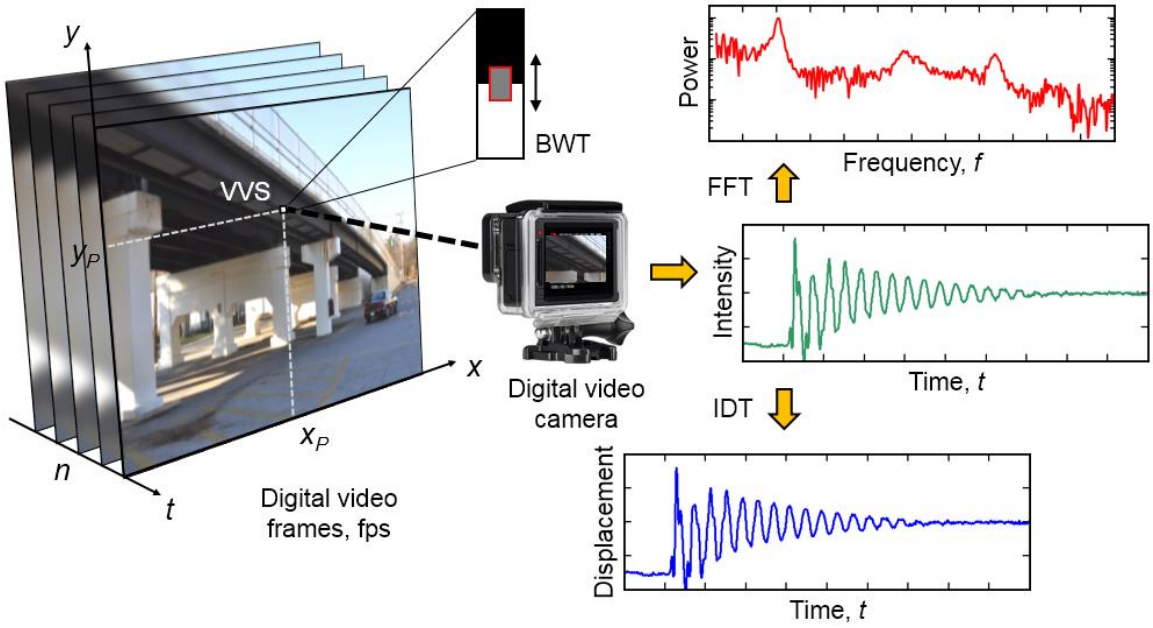

Figure 1. Illustration of the proposed methodology to measure structural vibrations using Eulerian-based virtual visual sensors (VVS). Acronyms: BWT = black-and-white target, FFT = Fast Fourier transform, IDT = intensity-to-displacement transform.

2 Background and Theory

As we discussed in [11], [12], change of intensity observed by our Eulerian-based virtual visual sensor (VVS) did previously not directly correspond to a physical quantity such as displacement, velocity, or acceleration. In this study, we evaluate the use of simple printed black-and-white targets (BWT) that allow the measurement of actual dynamic displacements, as visualized in Fig. 2. For an ideal BWT target observed in a digital video with dimensions L_t x W_t (pixel x pixel), the

pattern colors are represented by the minimum and maximum intensity values ($I_{min.}$ and $I_{max.}$, respectively) corresponding to 0 (= black) and 255 (= white), respectively. The displacement varies linearly with VVS patch intensity, $I_p(t)$:

$$I_p(t) = \frac{(I_{max} - I_{min})}{L_p} x(t) + n_p(t) \quad (1)$$

where $I_p(t)$ is the average pixel intensity across the patch area, $A_p = W_p$ x L_p (pixel x pixel) for a frame at time instant, t (sec), $x(t)$ (pixel) measured displacement, and L_p (pixel) is the length of the patch. It is assumed that intensity across the width of the patch, W_p (pixel) is constant and it therefore does not appear in Eq. (1). It should be noted that the patch length, L_p (pixel) should be large enough to account for the maximum displacement amplitude, A (pixel), i.e. $L_p > A$. At the same time, the length of the target, L_t (pixel) needs to be able to accommodate for the patch length, L_p (pixel), i.e. the target cannot leave the patch, otherwise the relationship becomes non-linear. Finally, there is no perfect BWT target (with perfect black (I = 0) or white (I = 255) intensity values) in a real setting and measurement noise is always present. The total average noise of the patch, $n_p(t)$ can be defined as:

$$n_p(t) = \frac{1}{N} \sum_{i=1}^{N} n_i(t) \quad (2)$$

where N is the total number of pixels in the VVS patch and n_i is the noise present in pixel i.

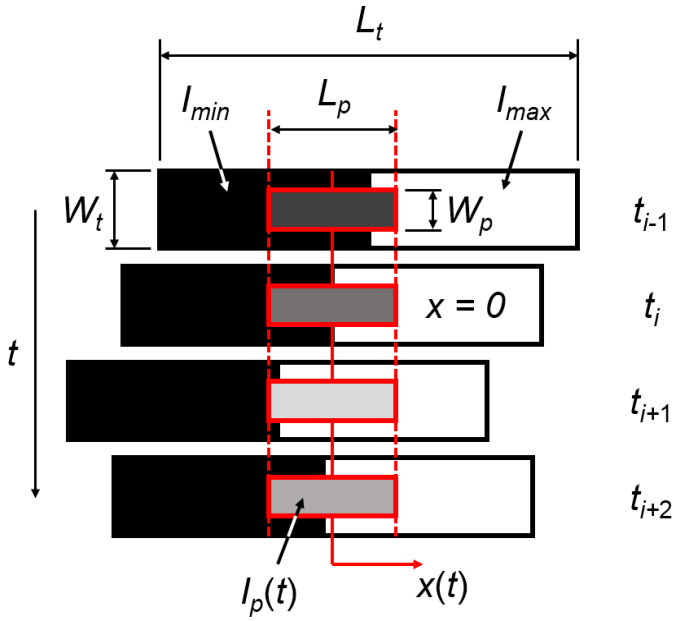

Figure 2. Illustration of the VVS measurement process using a black-and-white target (BWT): the target, which is attached to the vibrating structural element, moves in the *x*-direction relative to a fixed patch of pixels, i.e. having Eulerian-coordinates, as a function of time, *t*.

As an alternative to Eq. (1), VVS patch intensity, $I_p(t)$ can also be computed as the average intensity value of all pixels across the patch area, A_p:

$$I_p(t) = \frac{1}{N}\sum_{i=1}^{N} I_i(t) \tag{3}$$

where N is the total number of pixels in the VVS patch and I_i is the intensity value of pixel i.

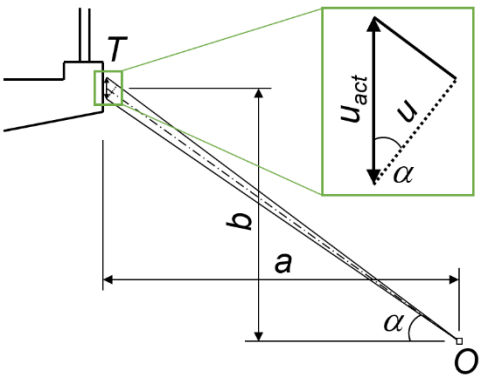

Figure 3. Illustration for the case where the camera is not oriented perpendicular to the displacement component of interest, u_{act}. *O* denotes the camera location and *T* the center location of the target mounted to the vibrating structure. *a* and *b* represent horizontal and vertical distance between the camera and the center of the target.

In order to correlate the observed intensity values to actual displacement, a calibration constant, *B* (mm/pixel) needs to be determined. This is done by dividing the actual length of the BWT (mm) by the corresponding number of pixels (pixels) observed from a selected frame of the video. For the case where the camera is not oriented perpendicular to the displacement component of interest, i.e. when $b \neq 0$, a geometric correction factor, *C* (unitless) applies. This factor is calculated based on the location of the camera (*O*) and the center location of the target (*T*), as illustrated in Fig. 3:

$$C = \frac{1}{\cos\left[\tan^{-1}\left(\frac{b}{a}\right)\right]} \tag{4}$$

Motion observed at angles ≠ 90 Degrees about the axis aligned with that motion (in our case vertical) are not affected in any significant manner and are thus not considered.

Considering that $I_p(t)$ is known and by using the calibration constant, B (mm/pixel) and the geometric correction factor, C, the actual dynamic displacement of the target, $u_{act}(t)$ can be computed using the following relationship:

$$u_{act}(t) = B \cdot C \cdot I_p(t) \text{ (mm)} \tag{5}$$

Changing lighting conditions affect the measured intensity values and thus introduce an error in the prediction of $u_{act}(t)$. This is really only a problem for long-term measurements (e.g. for SHM applications) but can be addressed by continuously normalizing the difference of the measured intensity values on the target ($I_{max} - I_{min}$) when lighting conditions change. For short-term measurements (e.g. annual impact or load tests) where the test time can be selected accordingly, this effect is negligible.

The presence of noise may require implementation of a noise reduction technique. Fortunately, for a BWT the averaging process (expressed by Eqs. (1) and (3)) by itself helps reducing the noise, i.e. the power of the noise reduces directly with the number of pixels in the patch, N. Assuming that the noise is independent of the signal and can be represented by a stationary process, we arrive at:

$$\sigma^2(I_p) = \frac{(I_{\max} - I_{\min})^2}{L_p^2}\sigma^2(x) + \frac{\sigma^2(n_p)}{N} \tag{6}$$

Eq. (6) relates the size of the VVS patch and the power of the noise and the signal. As can be seen from the second term of the right hand side of Eq. (6), as the number of pixels increases the power of the noise decreases. However, increasing the length of the patch will have the same effect on the power of the signal, hence keeping the length as short as possible and the width as large as possible will maximize the *SNR*. Substituting *N* for W_pL_p in Eq. (6), which is *width* x *length* of the patch, we can get the following expression for the signal-to-noise ratio (SNR):

$$SNR = \frac{\frac{\left(I_{\max} - I_{\min}\right)^2}{L_p^2}\sigma^2(x)}{\frac{\sigma^2(n_p)}{W_pL_p}} = \frac{W_p}{L_p}\left(I_{\max} - I_{\min}\right)^2 \frac{\sigma^2(x)}{\sigma^2(n_p)} \quad (7)$$

Eq. (7) shows that in order to reach the maximum *SNR* one has to maximize the W_p-to-L_p ratio keeping in mind that L_p should be able to cover the maximum displacement amplitude, *A*, as discussed earlier. For a specific camera and lighting conditions, the pixel noise power can be assumed constant and the appropriate size of the patch can be specified based on the desired *SNR*. The other factor that should be discussed in Eq. (7) is the second factor, $\left(I_{\max} - I_{\min}\right)$, which has a more significant effect on the *SNR*. It can be concluded from Eq. (7) that the higher the contrast between black and white in the target, the higher the *SNR* will be.

3 Experiments

3.1 Laboratory Setup and Instrumentation

A laboratory-scale three-degree-of-freedom structural system (Total height = 610 mm (2 ft) as shown in Fig. 4 (d) was used to evaluate the accuracy of the methodology proposed in Section 2.

177 The structure was excited by introducing random initial displacements at two locations on the
178 structure by hand followed by a sudden release to initiate free vibration. A digital camera (GoPro
179 Hero 3, shown in Fig. 4 (c))) capturing the free vibration response was located 305 mm (1 ft) away
180 from the structure. The displacement of the first floor was also measured using a 12.7 mm (0.5 in)
181 amplitude potentiometer (Fig. 4 (b)) connected to a high-speed data acquisition system (Fig. 4 (a))
182 using a sampling frequency of 1200 Hz. The frame rate of the digital camera was 60 frames per
183 seconds (fps).
184

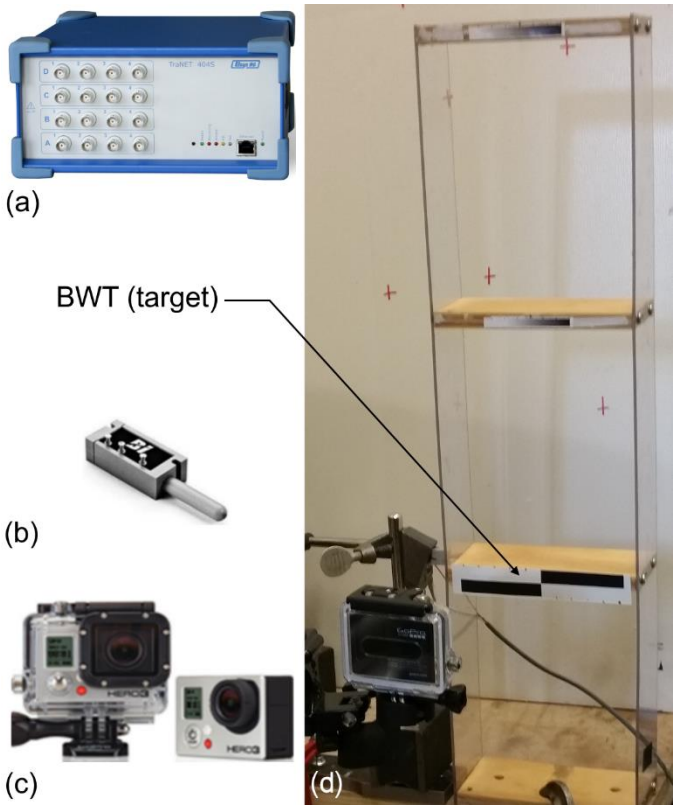

185

186 **Figure 4.** Experimental setup: (a) high-speed data acquisition system, (b) potentiometer to
187 measure displacements at the first story mass, (c) digital camera to collect VVS data, and (d)
188 three-degree-of-freedom laboratory structure.
189

190 **3.2 Data Acquisition and Data Preprocessing**

In order to compare the two measured signals, two steps have to be taken: (1) synchronization of the signals in the time domain and (2) multiplication of the measured signals by their appropriate calibration factors to obtain actual displacement from the measured data. It is good to mention that the $\left(I_{\max} - I_{\min}\right)$ value was assumed to be constant, which proved to be a correct assumption based on the data. Also the calculation of this value was based on the average of a black and white patch of pixels on the target that was taken from a snapshot of the videos. For step (1), both camera and potentiometer data were interpolated linearly to two equivalent 3000 Hz signals. Based on the maximum correlation between the two signals, the time lag between the two signals was calculated and one of the signals shifted so that they had a common time axis. In order to achieve actual displacement for step (2), the potentiometer was calibrated against a precision height gage. The mean calibration factor was found to be 1.257 mm/V (0.0495 in/V). For the camera intensity data, the known target length, L_t was measured in a video frame in terms of pixels, which produced a mean calibration factor of 0.279 mm/pixel (0.011 in/pixel).

In addition to the independent application of calibration factors as described above, it was also possible to multiply the VVS intensity data by a factor that minimizes the second norm of difference, or error, between the two measurements. This case represents the optimal estimate of the displacement for the VVS, assuming the potentiometer represents an accurate reference measurement. Obviously, in a real life scenario only the first approach can be used where a calibration factor has to be estimated from the video data. It should be noted that the potentiometer serves as the reference measurement but does not necessarily produce a more accurate displacement. This was particularly visible at the peak displacement points and is discussed in more detail in Section 4.1.

4 Results

4.1 Accuracy of Proposed Approach

Two VVS patch sizes, W_p x L_p = 40 x 50 and 40 x 100 pixels, were selected to study how the accuracy of the measurements change with the size of the VVS patch, A_p. Fig. 5 shows a snapshot of a video frame with the target and the two evaluated VVS patch sizes.

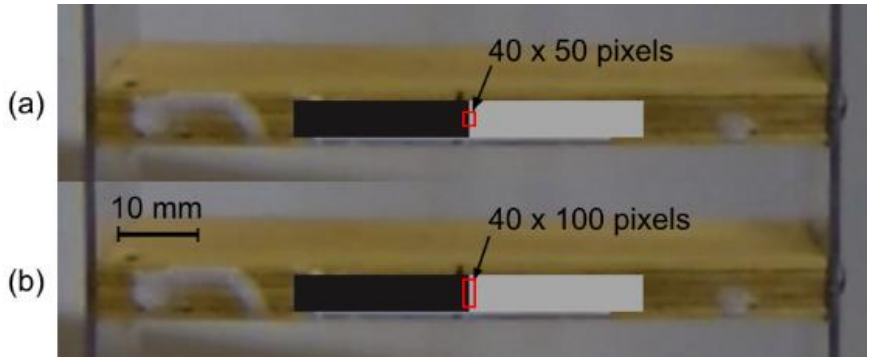

Figure 5. Photo of BWT target with two VVS patch sizes: (a) 40 x 50 pixel patch and (b) 40 x 100 pixel patch.

Fig. 6 shows a comparison of a sample measurement using independent calibration factors, as described in Section 3.2. As can be observed from Fig. 6 (a), the displacements measured by the VVS and the potentiometer are, qualitatively, in close agreement for both patch sizes. However, the inserts in Fig. 6 (a) reveal that the end of the signal of the 40 x 100-pixel patch resembles the potentiometer's measurement more closely. A direct correlation between the two measurements (Fig. 6 (b)) shows approximately a straight line with a slope of 0.95 and 0.92 with a squared correlation coefficient of 99.6 and 99.9% for the patch size of 40 x 50 and 40 x 100 pixels, respectively. The absolute prediction error at the 95% confidence level was determined by

measuring the distance between the 95% prediction limits shown in Fig. 6 (b) (red dotted lines) and found to be 0.12 and 0.24 mm (0.0047 and 0.0094 in) for the patch size of 40 x 50 and 40 x 100 pixels, respectively. Furthermore, in Fig. 6 (c), which shows the absolute value of the difference between the two measurements, less than 2% of the signal difference is greater than a pixel size and roughly 90% of the time the difference is less than half of a pixel size. It can further be observed that the difference shows distinct evenly-spaced peaks that are highest at the beginning of the signal. Also, they appear to coincide with the peak amplitudes of the signal. The difference is likely due to an error in the potentiometer measurement, when the direction of the displacement changes. Unfortunately, it was not possible for us to ascertain this claim completely. In the future, we plan to perform further laboratory tests using a laser vibrometer. Despite this uncertainty, our data shows that subpixel-level accuracy is achievable with high confidence. The actual difference in terms of noise can be observed by visually comparing the curves in Fig. 6 (c) between 4 and 6 s. The distribution of the error with mean, μ and standard deviation, σ is shown in Fig. 6 (d). It can be observed from the distribution of the signal difference that it appears to follow a Normal distribution, as assumed in Section 2.

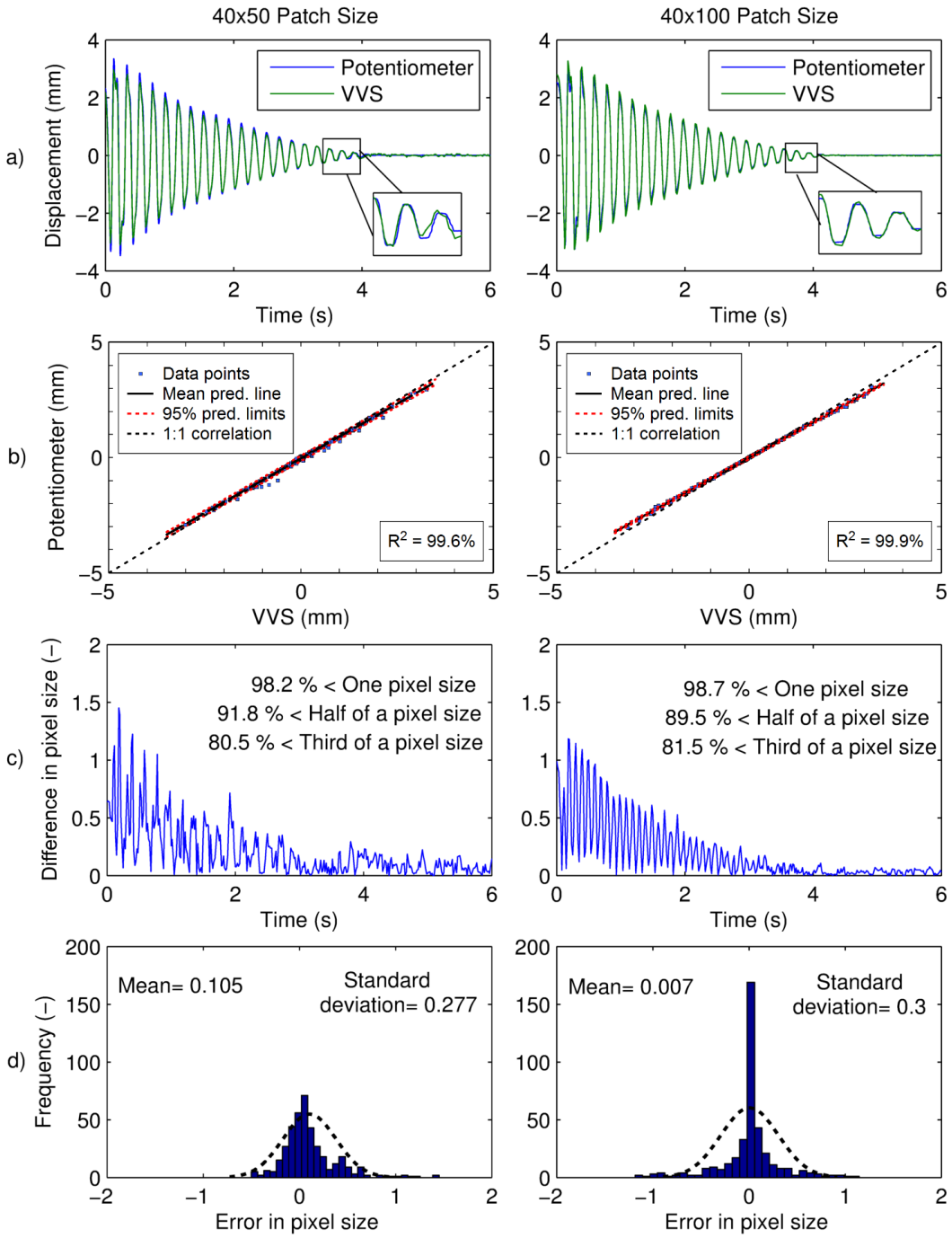

Figure 6. Comparison of results using independent calibration factors, 40 x 50 pixels (left column) and 40 x 100 pixels (right column): (a) Time history signals of VVS patch data and potentiometer, (b) correlation between the two measurements with regression lines, (c) absolute value of the difference between the two signals (errors), and (d) histogram of the errors.

Fig. 7 shows the case where the calibration factor for the VVS was optimized as discussed in Section 3.2. Fig. 7 (a) compares with Fig. 6 (a) while correlation plots shown in Fig. 7 (b) are even better compared to Fig. 6 (b). The slope of the prediction line in Fig. 6 (b) is 0.99 and 0.98 with a squared correlation coefficient of 99.5 and 99.9% for the patch size of 40 x 50 and 40 x 100 pixels, respectively. The absolute prediction error at the 95% confidence level, computed as described earlier, was found to be 0.26 and 0.11 mm (0.01 and 0.0043 in) for the patch size of 40 x 50 and 40 x 100 pixels, respectively. The maximum signal difference (Fig. 7 (c)) is reduced by almost half of a pixel size as compared to Fig. 6 (c). Comparing the patch sizes in Fig. 7 (d), it can be observed that the standard deviation of the pixel error has been significantly decreased from 0.23 pixels to 0.12 pixels for the 40 x 50-pixel patch compared to the 40 x 100-pixel patch, respectively. Also, with a confidence of more than 90%, the error in the smaller patch is less than one third of a pixel size while in the bigger patch it is less than one fifth of a pixel size. Again, this approach represents the case where the calibration factor for the VVS sensor was optimized by minimizing the difference between the two measurements.

In conclusion from Figs. 6 and 7, we have demonstrated that subpixel accuracy can be achieved with high confidence, even without implementing a computationally-expensive block matching algorithm, and that estimates of the dynamic displacement can be achieved in a laboratory setting with absolute prediction errors of approximately 0.25 mm (0.01 in).

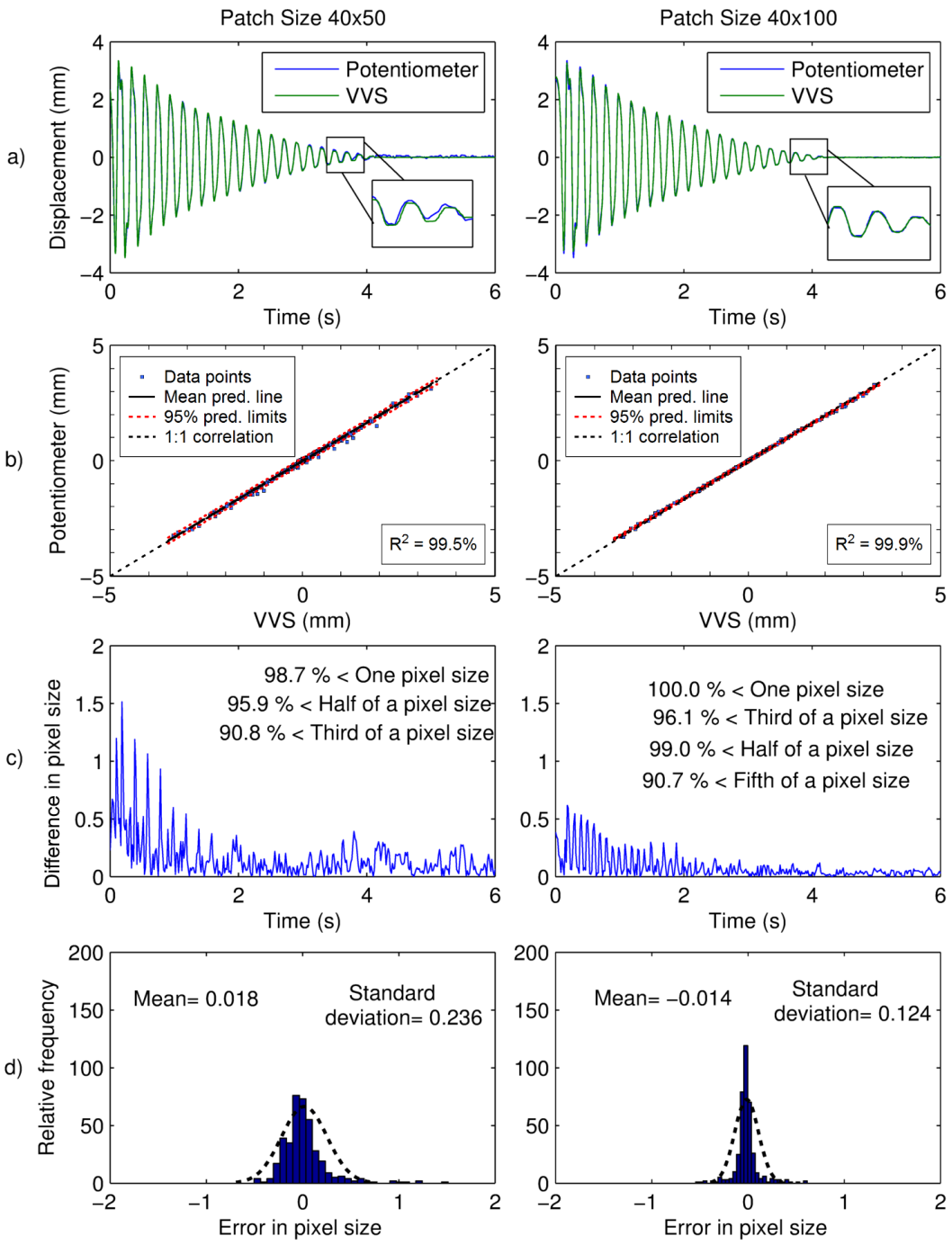

Figure 7. Comparison of results using calibration factors based on minimized difference between measurements, 40 x 50 pixels (left column) and 40 x 100 pixels (right column): (a) Time history signals of camera and potentiometer, (b) correlation between the two measurements with regression lines, (c) absolute value of the difference between the two signals (error), and (d) histogram of the error.

Table 1 summarizes the main results of the accuracy evaluation presented in this section. It can be seen that the larger VVS patch (40 x 100 pixels) was closer to the potentiometer reading compared to the smaller patch (40 x 50 pixels). For the displacements computed using the independent factors, the larger sized VVS patch was closer to the potentiometer measurement. However, the standard deviation of the difference for the larger patch remained the same because of the calibration issues explained earlier. While this type of comparison can likely not be performed in the field, as it would require an independent physical measurement of the displacement, it allowed us to isolate and study the calibration errors and the inherent irreducible noise using the proposed VVS.

4.2 Relationship of Noise and Patch Size

Fig. 8 (d) shows the relationship between patch noise and number of pixels in a VVS patch as defined theoretically by Eq. (7) and observed experimentally. As can be seen in Fig. 8 (a), the power of the noise is close to the theoretical values. Figs. 8 (b) and (c) show the distribution of the noise for one pixel and a patch of 10 x 10 pixels. As can be observed, the noise in the patch follows a Normal distribution and its power is one order of magnitude smaller than that for one pixel. Also, the SNR values approximately change linearly with the width to length ratio of the patch as predicted from Eq. (7). This validates the theoretical framework presented in Section 2.

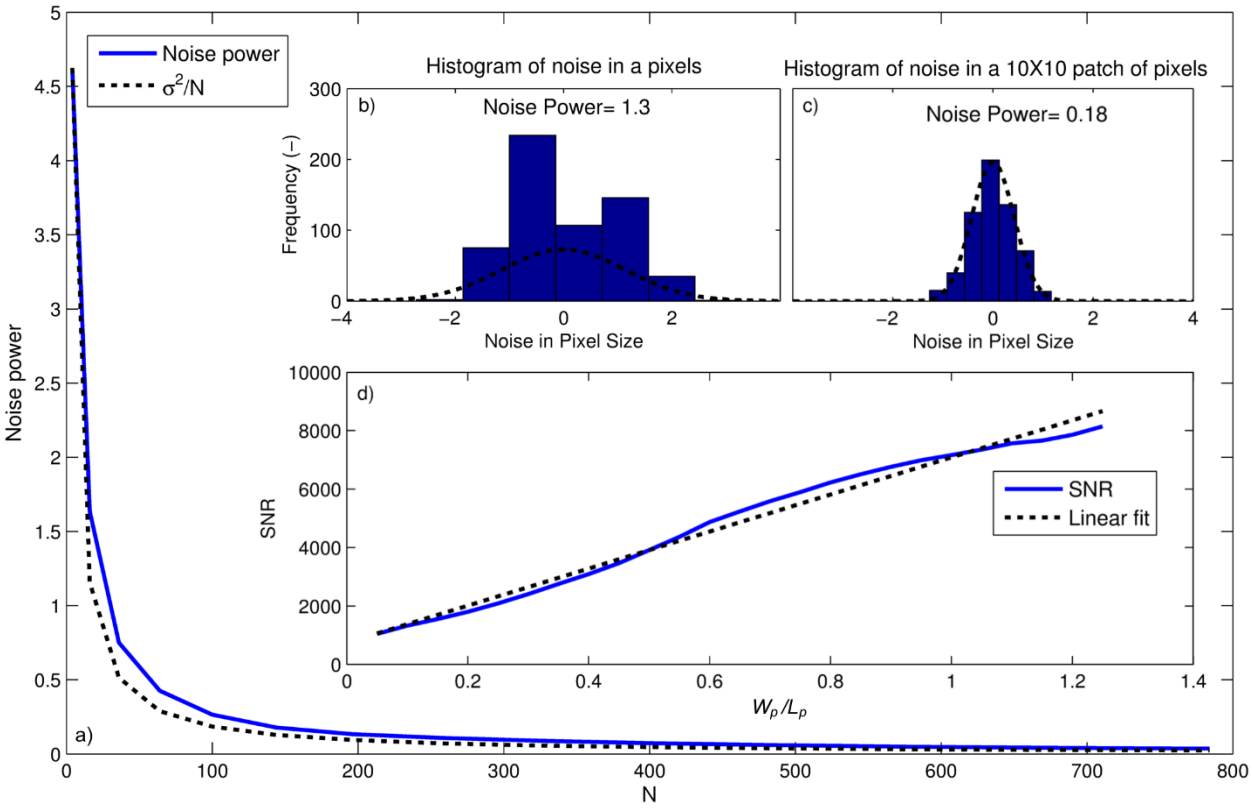

Figure 8. Noise power and the signal-to-noise ratio (SNR): (a) Power of the noise vs. the number of pixels in the VVS patch (*N*), (b) histogram of noise in one pixel, (c) histogram of noise in a 10 x 10-pixel patch, and (d) the SNR values vs. width over length of the patch.

4.3 Dynamic In-Service Load Test on the Streicker Bridge

In order to evaluate the applicability of the proposed methodology in a real-world scenario, the Streicker Bridge was tested dynamically with a black-white target (BWT) to compute displacement. Located on the Princeton University campus, the bridge has a unique design with a straight main deck section supported by a steel truss system underneath and four curved ramps leading up to the straight sections, as shown in Fig. 9. One of the ramps was instrumented with a fiber-optic measurement system during construction by Br. Branko Glisic from Princeton University [14]. For our test, we installed an off-the-shelf Canon EOS Rebel T4i camera with a

312 standard Canon EF 75-30mm zoom lens aimed at one of the ramps, to take a 60 fps video while a
313 number of volunteers jumped up and down on it. A VVS patch having 60 x 20 pixels was chosen
314 to compute displacements. As can be seen in Fig. 8, the VVS is located at a black-and-white edge
315 on a target mounted to the edge of the bridge slab. This target was set up by Dr. Maria Feng's
316 research team from Columbia University, who collected data for evaluation of their own video-
317 based monitoring methodology [15]. The relationships in Eqs. (1) and (5) were used to compute
318 the actual vertical dynamic displacement from the collected VVS patch. The calibration constant,
319 *B* was estimated from the target size as *17.3* (mm/pixel); the geometric correction factor, *C*
320 estimated to be *1.02*.
321

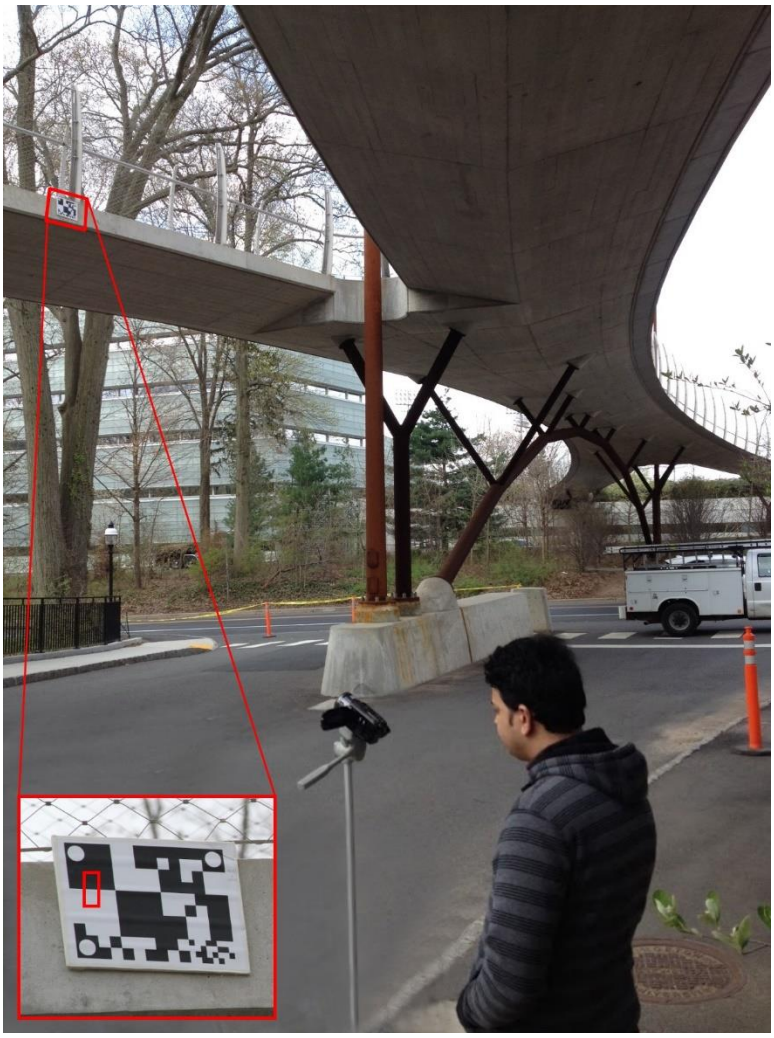

Figure 9. Photograph of the Streicker Bridge showing the measurement setup and the location of the VVS. The insert shows the location of the 60 x 20 pixel VVS patch (red rectangular). The target was installed by Dr. Maria Feng's research team from Columbia University [15].

The computed vertical displacement response of the ramp section due to the described dynamic forcing for a duration of 15 seconds is presented in Fig. 10. In our earlier paper we already reported that the natural frequencies for this same test were found to be the same as those measured by the fiber-optic measurement system [14]. Although we have no other physical measurement available to directly compare and verify our computed displacement, it is comparable in amplitude to what

the Columbia University team reported [15]. Also, the frequency peak is exactly the same as reported by the same group.

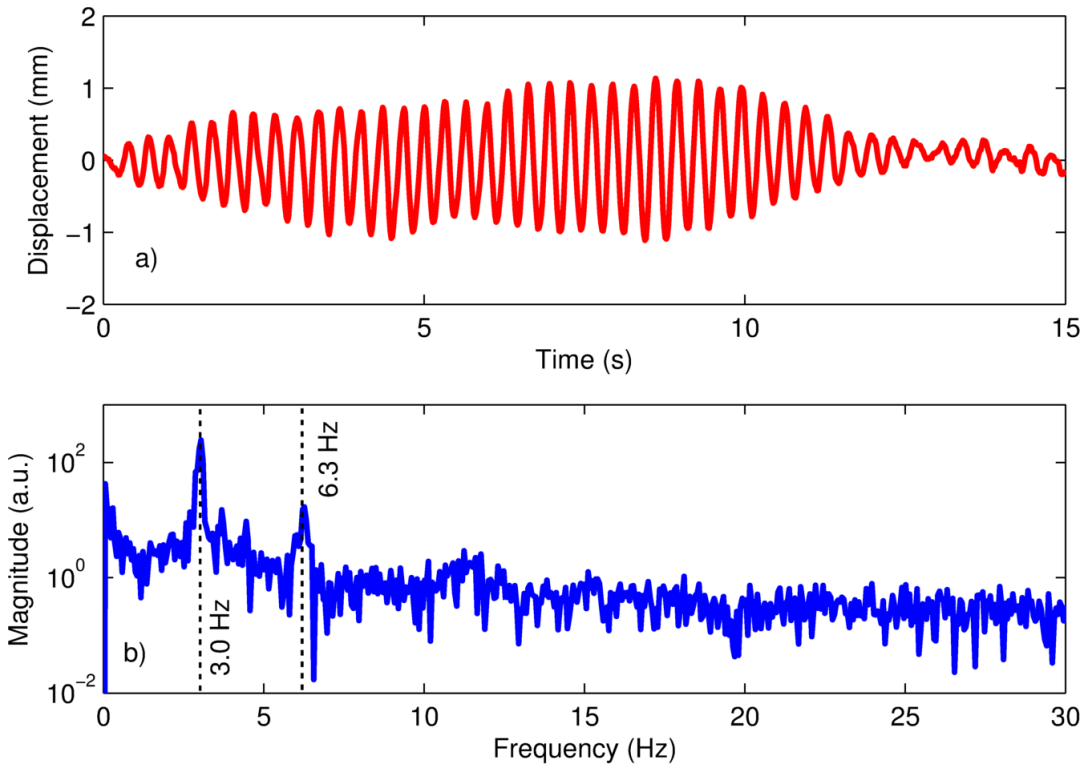

Figure 10. Results from the dynamic load test on the Streicker Bridge: (a) Computed actual vertical displacement time history and (b) frequency response of signal (a).

5 Discussion and Conclusions

The objective of this study was to evaluate the possibility of computing actual dynamic displacements using Eulerian-based virtual visual sensors (VVS) . This is based on the idea that either an edge of a vibrating structural element or a black-and-white target (BWT) can be monitored by a patch of pixels. The noise in the VVS sensor was found to be inversely related to the patch size. The following conclusions can be made from on our study:

- The use of BWT allows for accurate computation of dynamic displacements of a vibrating structural element comparable to the measurements from a potentiometer.
- The laboratory tests demonstrated that sub-pixel accuracy can be achieved similar to block matching algorithms. The absolute prediction error at the 95% confidence limit was found to be approximately 0.25 mm (0.01 in) relative to the reference measurement.
- The accuracy in the measurement of the displacement implies that change of intensity is highly sensitive to even tiny amounts of movement, which results in the fact that natural frequencies can be measured as proposed in [11]–[13] even if the displacement is much less than a pixel size.
- Our proposed approach also works in the field, as demonstrated by the measurements of the Streicker Bridge. A direct validation was not possible since no other physical displacement data was available, which is typically the case for field measurements. However, the frequency content of the signal has already been verified in [18] and the displacement amplitude as well as the frequency peak is comparable to what the team from Columbia University found [15].
- The influence of camera movement and changes in lighting conditions need to be addressed further in future research.

Acknowledgments

The support by a Center for Advanced Infrastructure and Transportation University Transportation Research (CAIT-UTC) grant (Contract No. DTRT12-G-UTC16) and the Department of Civil and Environmental Engineering at the University of Delaware for this study is greatly appreciated. We further thank our colleague Prof. Branko Glisic, who facilitated access for the field test on the Streicker Bridge located on Princeton University's campus. Finally, we would like to thank Dr.

Nakul Ramanna for assisting with the field test, Dr. Maria Feng and her team from Columbia University for allowing us to use their target, and Mr. Marcus Schwing for his expertise in photo editing.

References

[1] A. Deraemaeker and K. Worden, *New trends in vibration based structural health monitoring*. 2012.

[2] S. W. S. Doebling, C. R. C. Farrar, M. B. M. Prime, and D. W. D. Shevitz, "Damage identification and health monitoring of structural and mechanical systems from changes in their vibration characteristics: a literature review," 1996.

[3] C. R. Farrar and K. Worden, "An introduction to structural health monitoring.," *Philos. Trans. A. Math. Phys. Eng. Sci.*, vol. 365, no. 1851, pp. 303–315, 2007.

[4] H. H. Nassif, M. Gindy, and J. Davis, "Comparison of laser Doppler vibrometer with contact sensors for monitoring bridge deflection and vibration," *NDT E Int.*, vol. 38, no. 3, pp. 213–218, Apr. 2005.

[5] B. D. Lucas and T. Kanade, "An Iterative Image Registration Technique with an Application to Stereo Vision," *IJCAI*, vol. 130, pp. 674–679, 1981.

[6] H. Leclerc, J. Périé, S. Roux, and F. Hild, "Integrated digital image correlation for the identification of mechanical properties," *Comput. Vision/Computer Graph. ...*, pp. 161–171, 2009.

[7] R. C. Oats, D. K. Harris, T. (Tess) M. Ahlborn, and H. A. de Melo e Silva, "Evaluation of the Digital Image Correlation Method as a Structural Damage Assessment and Management Tool," in *Transportation Research Board 92nd Annual Meeting*, 2013.

[8] I. B. Mohammad Bolhassani, Satish Rajaram, Ahmad A. Hamid, Antonios Kontsos, "Damage detection of concrete masonry structures by enhancing deformation measurement using DIC," in *Nondestructive Characterization and Monitoring of Advanced Materials, Aerospace, and Civil Infrastructure X, SPIE*, 2016.

[9] C. A. Murray, W. A. Take, and N. A. Hoult, "Measurement of vertical and longitudinal rail displacements using digital image correlation," *Can. Geotech. J.*, vol. 52, no. 2, pp. 141–155, Feb. 2015.

[10] Y.-Z. Song, C. R. Bowen, A. H. Kim, A. Nassehi, J. Padget, and N. Gathercole, "Virtual visual sensors and their application in structural health monitoring," *Struct. Heal. Monit.*, vol. 13, no. 3, pp. 251–264, Feb. 2014.

[11] T. Schumacher and A. Shariati, "Monitoring of structures and mechanical systems using virtual visual sensors for video analysis: fundamental concept and proof of feasibility.," *Sensors (Basel).*, vol. 13, no. 12, pp. 16551–64, Jan. 2013.

[12] A. Shariati, T. Schumacher, and N. Ramanna, "Eulerian-based virtual visual sensors to detect natural frequencies of structures," *J. Civ. Struct. Heal. Monit.*, vol. 5, no. 4, pp. 457–468, 2015.

[13] A. Shariati and T. Schumacher, "Oversampling in virtual visual sensors as a means to recover higher modes of vibration," in *AIP Conference Proceedings (Proceedings of QNDE 2014, July 20-25, Boise, ID.)*, no. Dic, pp. 1–7.

[14] B. Glisic, J. Chen, and D. Hubbell, "Streicker Bridge: a comparison between Bragg-grating long-gauge strain and temperature sensors and Brillouin scattering-based distributed strain and temperature sensors," in *SPIE Smart Structures and Materials + Nondestructive Evaluation and Health Monitoring*, 2011, p. 79812C–79812C–10.

[15] D. Feng, M. Q. Feng, E. Ozer, and Y. Fukuda, "A Vision-Based Sensor for Noncontact Structural Displacement Measurement.," *Sensors (Basel).*, vol. 15, no. 7, pp. 16557–75, Jan. 2015.

419 **Table1.** Summary table of accuracy evaluation.

	Independent calibration factors (see Fig. 6)		Minimization of signal difference (see Fig. 7)	
Size of the patch	40 x 50	40 x 100	40 x 50	40 x 100
Correlation Coefficient	0.998	1.000	0.998	1.000
Maximum difference in pixel size	1.5	1.2	1.5	0.6
Mean of the difference	0.105	0.007	0.018	-0.014
Standard deviation of the difference	0.277	0.300	0.236	0.124

420